Chinese Chemical Letters 36 (2025) 109785

Contents lists available at ScienceDirect

Chinese Chemical Letters

journal homepage: www.elsevier.com/locate/cclet

Smartphone-assisted electrochemiluminescence imaging test strips towards dual-signal visualized and sensitive monitoring of aflatoxin B1 in corn samples

Miao-Miao Chen[a,b,e], Min-Ling Zhang[e], Xiao Song[e], Jun Jiang[a,b], Xiaoqian Tang[a,b,c,d], Qi Zhang[a,b,c,d], Xiuhua Zhang[e], Peiwu Li[a,b,c,d,*]

[a] Key Laboratory of Biology and Genetic Improvement of Oil Crops, Ministry of Agriculture and Rural Affairs; Laboratory of Risk Assessment for Oilseed Products (Wuhan), Quality Inspection and Test Center for Oilseed Products, Oil Crops Research Institute, Chinese Academy of Agricultural Sciences, Wuhan 430062, China
[b] Food Safety Research Institute, Hubei University, Wuhan 430062, China
[c] Hubei Hongshan Laboratory, Wuhan 430070, China
[d] Xianghu Laboratory, Hangzhou 311231, China
[e] College of Chemistry and Chemical Engineering, Hubei University, Wuhan 430062, China

ARTICLE INFO

Article history:
Received 25 February 2024
Revised 17 March 2024
Accepted 17 March 2024
Available online 18 March 2024

Keywords:
Electrochemiluminescence imaging
Test strips
Nanomaterials
Dual-signal outputs
Aflatoxin B1
Food safety

ABSTRACT

Aflatoxins B1 (AFB1) contamination in agro-food holds great threaten to human and animal health. Conventional test strips for rapid AFB1 visualized monitoring remains challenged by improvement of sensitivity and matrix interference resistance. In this case, we developed a portable electrochemiluminescence (ECL) imaging test strip with dual-signal outputs for AFB1 quantification in corn samples. Ru-PEI@SiO_2@Au nanospheres were synthesized for bonding with anti-AFB1 antibody and then colorimetrical signal-reported on test line through the capillary flow at strips. Meanwhile, ECL imaging signal of the constructed carbon-ink-based working electrode on polyvinyl chloride substrate of strips was exported under an applied potential of 1.25 V. The whole ECL test strips not only endowed convenient colorimetric responses but guaranteed quick-witted ECL image distinguishment even at extremely low AFB1 content. The detection limit of this ECL imaging-integrated mode was 10-fold lower than that of only colorimetric mode. Furthermore, satisfactory selectivity, reliability and practicability of the as-proposed ECL test strips were demonstrated. This work offered a promising platform for on-site, accurate and sensitive detection of pollutants in foods.

Mycotoxins are toxic secondary metabolites produced by fungi of different genera including *Aspergillus*, *Penicillium* and *Fusarium*, which potentially contaminates crops, food products and animal feed at every stage of food supply chain, especially under conditions of high temperature and humidity [1–3]. Mycotoxin contamination holds a significant threat in agriculture and food safety due to their adverse effects on human and animal health. Thereinto, aflatoxins B1 (AFB1) classified as a Group 1 human carcinogen by the International Agency for Research on Cancer (IARC) has attached great concerns and strictly limited in China's national standard on food safety (maximum permissible of 5.0 μg/kg in beans or 5.0–20 μg/kg in grain, GB 2761–2017). European Commission has also stringently set 0.5 ng/mL as Maximum Residue Level for AFB1 in edible food and milk [4]. Besides, the heat-stable and lipophilic properties made AFB1 very difficult to be detoxicated or removed. Therefore, developing rapid and reliable methods for AFB1 contamination tracing is crucial for ensuring food safety and preventing the consumption of contaminated products [5,6]. Massive efforts had been given rise for establishing rapid and on-site determinate of AFB1, including enzyme-linked immunosorbent assay, point-of-care sensors and immunochromatography [7]. Traditionally, paper-based lateral flow immunochromatographic (LFI) assay employed colorimetric or fluorescent labels to output the visual interpretation of test line for rapid determination [8]. This method possessed advantages of portability, simplicity, short testing time and low cost, which has been widely applied for medical diagnosis and food safety risk assessment [9]. However, towards ultra-trace monitoring of AFB1, the limitations of inadequate sensitivity or poor quantitative discrimination is still a challenge.

* Corresponding author.
E-mail address: peiwuli@oilcrops.cn (P. Li).

https://doi.org/10.1016/j.cclet.2024.109785
1001-8417/

Erenow, diverse techniques-coupled LFI assays have been progressively investigated to construct versatile strip tests for mycotoxin quantification, such as fluorescent LFI [10,11], photothermal LFI [12,13] and surface-enhanced Raman scattering-based LFI [14,15] assays. Though these devices effectively improved the measurement sensitivity in a degree, there are still some deficiencies, such as background light interference (autofluorescence and scattered light) or insufficient environmental stability. Notably, inspired by electrochemical sensors with controllable potential, good sensitivity and miniaturization, the integration of three-electrode system and LFI assay for constructing electrochemical (EC) or electrochemiluminescence (ECL) test strips to quantify analytes has exuberantly sprung up recently [16–19].

As a derivative of EC method, ECL process undergoes the generation of the excited state of luminescent species from electron transfer reactions at electrode and then emission light [20,21]. Especially that was superior to EC sensors, ECL assay enabled directly visualized imaging, superior reproducibility and dramatically improved sensitivity, especially for food analysis [22,23], offering an energetic candidate coupled with LFI assay for rapid detection. However, despite the desirable progress in the fabrication of screen-printed electrode-based ECL-LFI assay for protein analysis, unbefitting mass transfer interface between the stiffly inserted electrode and strip as well as expensive cost considerably limits potential applications [16,17]. Therefore, it is imperative to design and construct a portable and high-performance ECL test strips capable of AFB1 rapid monitoring, which has not been reported.

Hence, we developed an ECL test strip compatible with smartphones for dual-signal visualized detection of tracing AFB1 contamination in food samples (Fig. 1). This device was fabricated by directly patterning carbon ink onto the surface of polyvinyl chloride (PVC) substrate of LFI strips first. Then Ru-PEI@SiO_2@Au nanoparticles as signal probes were synthesized and connected to antibody-AFB1 for competitive immune reaction with AFB1-BSA antigen on test line (T-line) of strips. Attractively, Ru-PEI@SiO_2@Au probes not only endowed ECL test strips colorimetric answer under high levels of AFB1 target but guaranteed strong ECL image distinguishment produced by Ru-PEI lumiphore-coreactant pairs even extremely low AFB1 content. After a series of optimizations, the as-proposed ECL test strips finally received accurate and sensitive performance and across a wide dynamic range within 15 min toward AFB1 detection. This dual-signal ECL test strip allowed sensitive AFB1 determination in real corn samples, indicating its practicality for rapid food safety monitoring.

As illustrated in Fig. 2A, a hollowed-out self-adhesive pattern carved by a cutting plotter was adhered to PVC surface. Subsequently, conductive carbon ink was well-distributed painted onto the pattern area and then pattern was peeled off. After coating a LFI strips thereon, carbon ink-based three-electrode bands were successfully adhered on the PVC to form an all-in-one ECL test strip. The position of working electrode band was vertically aligned with that of T line on the LFI strip.

The surface morphologies and properties of the as-prepared ECL test strip were investigated by Scanning electron microscopy (SEM), contact Angle and Raman spectroscopy measurements. Compared to bare PVC with a glossy and hydrophobic surface (Fig. S1 in Supporting information), a carbon coating layer is uniformly and completely distributed on the modified electrodes (Fig. 2B), providing a relatively large specific area and desirable conductivity. The hydrophobic interface has a water contact angle of 102.3° (Fig. 2B, inset), which isolated the electrode from flow channels and made flow channels unaffected by the electrode, ensuring the fluidity of liquids in ECL test strips. The detailed information on the modified carbon coating electrode was analyzed by Raman spectroscopy (Fig. 2C). Two peaks at 1350 cm^{-1} and 1575 cm^{-1} assigned to D band and G band, respectively, representing the amorphous carbon and sp^2-hydridized carbon network.

The effect of wetting nitrocellulose (NC) membrane on electrochemical performance of the ECL test strip was deeply studied by electrochemical impedance spectroscopy (EIS) and cyclic voltammetry (CV). Commonly, the Nyquist plot of EIS displayed an incomplete semicircle in the high-frequency range and a non-linear line in the low-frequency region. The diameter of the semicircle indicated the charge-transfer resistance (R_{ct}) of the electrode interface. As displayed in Fig. 2D, the carbon ink modified PVC three-electrode system showed a R_{ct} of 215 Ω (curve a). After LFI integration, the whole strip had a slightly increased resistance of 343 Ω (curve b) resulted from the coverage of wetting NC membrane on the working electrode surface. Furthermore, the electroactive area of ECL test strip was explored by CV scans at different rates ranged from 50 mV/s to 200 mV/s. With the scan rate accelerated, the anodic and cathodic peak currents both increased accordingly (Fig. 2E). An acceptable linear dependence of peak current values to $\nu^{1/2}$ indicated a diffusion-controlled process (Fig. 2F). The effective working area was calculated using the Randles-Sevcik equation to be 0.088 cm^2. Under continuous scanning at 100 mV/s, a pair of peaks for ECL test strip exhibited high consistency and stability even after the 50th cycle, indicating a *quasi*-reversible electrochemical behavior (Fig. 2G), providing a steady redox reaction interface in all-in-one device.

Taken these findings together, the carbon ink printed PVC three-electrode system perfectly integrated with LFI strip and competently achieved electrochemical process to meet the further application on ECL image. As depicted schematically in Fig. 3A, Ru-PEI complex was fabricated by covalently bonding multi-carboxyl $[Ru(dcbpy)_3]^{2+}$ and amino-rich PEI and then was doped into silica

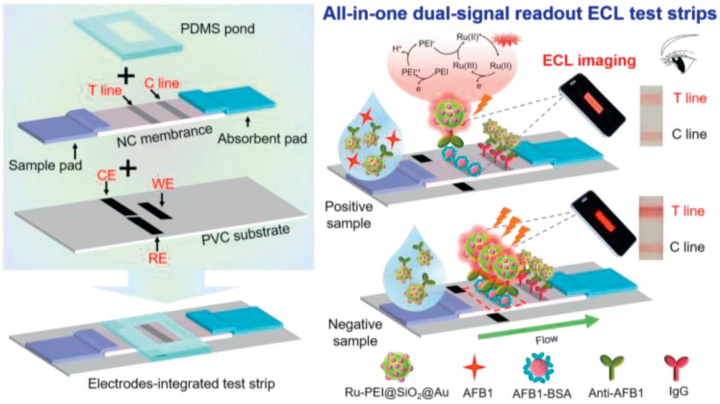

Fig. 1. Schematic diagram of the fabrication and detection process of the as-proposed dual-signal readout ECL test strips.

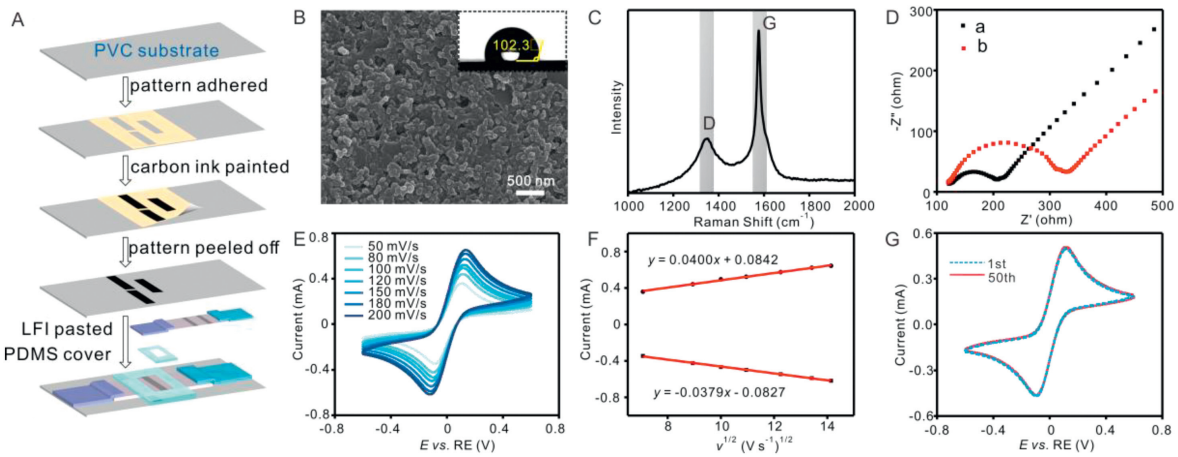

Fig. 2. (A) The construction progress of ECL test strips. (B) Scanning electron microscope (SEM) image and water contact angle (inset) of the surface of carbon ink-modified PVC. (C) Raman spectrum of carbon ink electrode surface. (D) Electrochemical impedance spectroscopy (EIS) profiles of (a) the carbon ink modified PVC three-electrode system and (b) all-in-one ECL test strip. (E) Cyclic voltammograms of all-in-one ECL test strips under different scan rates. (F) Plots of anodic and cathodic peak currents *vs.* the square root of the scan rate ($v^{1/2}$). (G) CV current signals of all-in-one ECL test strip scanned for continues 50 cycles (scan rate of 100 mV/s). All the EIS and CV measurements were executed in 0.1 mol/L KCl containing 50 mmol/L $[Fe(CN)_6]^{3-/4-}$ solution.

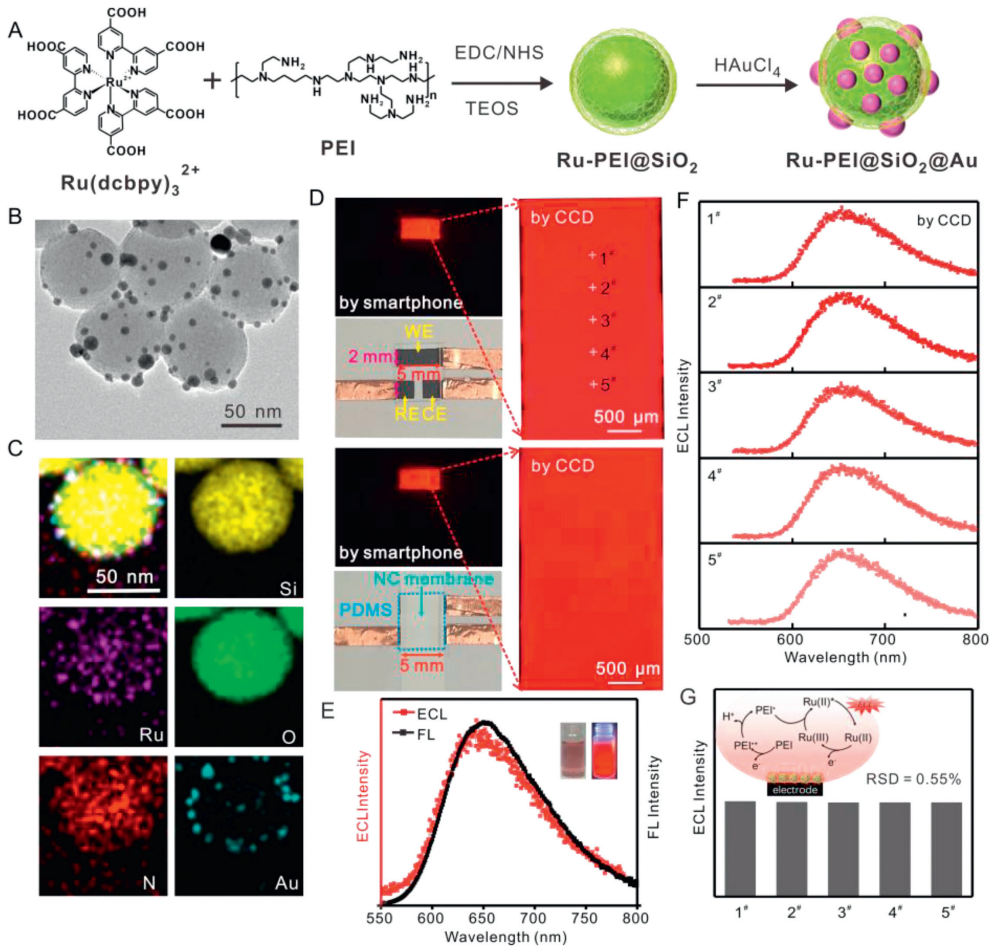

Fig. 3. (A) Diagram of synthesis process, (B) transmission electron microscopy (TEM) image and (C) energy dispersive X-ray spectroscopy (EDX) mapping images of Ru-PEI@SiO_2@Au. (D) ECL images recorded by smartphone or CCD camera before (top) and after (down) covering the three-electrode PVC substrate with a strip tested in 50 μL 0.1 mol/L PBS (pH 7.5) solution containing Ru-PEI@SiO_2@Au. (E) ECL-wavelength spectrum and FL spectrum of Ru-PEI@SiO_2@Au dispersions. Insert showed the photographs of Ru-PEI@SiO_2@Au dispersions under visible (left) and UV-light ($\lambda = 365$ nm, right). (F) ECL-wavelength spectra and (G) the corresponding ECL intensities of different five points on the ECL test strips.

to gain Ru-PEI@SiO_2 nanospheres (TEM, Fig. S2 in Supporting information) with a diameter of 60.9 ± 0.6 nm (Fig. S3A in Supporting information). After *in-situ* reduction of $HAuCl_4$, HRTEM image clearly showed that Au nanoparticles (Au NPs) were distributed outside of Ru-PEI@SiO_2 to form spherical and monodispersed Ru-PEI@SiO_2@Au nanocomposites (Fig. 3B) with an average diameter of 62.6 ± 0.7 nm (Fig. S3B in Supporting information). Meanwhile, elemental mapping clarified the coexistence of Si, O, Ru, N, and Au elements in the nanosphere (Fig. 3C). Otherwise, with the decoration of silica and Au NPs step by step, the zeta potential of 29.3 mV for Ru-PEI was gradually changed to 16.2 mV for Ru-PEI@SiO_2 and 9.6 mV for Ru-PEI@SiO_2@Au (Fig. S4A in Supporting information). This was ascribed to positively charged Au NPs were linked onto the surface of Ru-PEI@SiO_2 by the strong electrostatic interaction. UV–vis and fluorescence spectra of different nanomaterials were presented in Figs. S4B and C (Supporting information). Comparing with two characteristic absorption peaks at around 285 nm (an intra-ligand transition, $\pi \rightarrow \pi^*$) and 460 nm (the metal-to-ligand charge transfer) of free $Ru(dcbpy)_3^{2+}$ (Fig. S4B in Supporting information), the absorption spectrum of Ru-PEI@SiO_2@Au had a very small red-shift (~2 nm) and an extra peak of Au NPs emerged at around 530 nm. The fluorescence emission peak of Ru-PEI@SiO_2@Au showed a blue-shift about 15 nm in contrast to that of $Ru(dcbpy)_3^{2+}$ (Fig. S4C in Supporting information), which was induced by the interaction between SiO^- groups and $Ru(dcbpy)_3^{2+}$ dye. These characteristics manifested the successful preparation of Ru-PEI@SiO_2@Au luminophores.

ECL imaging and spectra signal acquisitions were implemented by directly instilling Ru-PEI@SiO_2@Au dispersion liquid onto three-electrode PVC substrate and covered test strips and PDMS pond thereon. Fig. 3D reveals the ECL images recorded by CCD camera over the same region of interest of the working electrode (WE) area before and after covering with test strip when an anodic potential of 1.25 V was applied to electrode in a PBS solution. Consistently, a homogeneous and bright red ECL emitted light was visualized, revealing the robust ECL image ability of the test strips. A continuous ECL spectral scanning at random fixed a point indicated that the ECL peak signal occurred at about 652 nm, which was approximate to that of FL spectrum (Fig. 3E) of Ru-PEI@SiO_2@Au nanocomposites, indicating ECL emission arise from the excited state of Ru(II) to ground state. Notably, almost perfectly consistent ECL spectra shapes of the picked five points on an all-in-one ECL test strip (Fig. 3F) were received. The synchronous recording ECL intensity values displayed high stability with RSD value of 0.55% (Fig. 3G). As schematically shown in Fig. 3G (inset), the electrochemical oxidation of Ru(II) species and PEI concurrently occurred on the electrode surface to produce Ru(III) and a radical cation. Then after a deprotonation process, the excited state Ru(II)* was generated through a intramolecular annihilation, which returned the ground state together with ECL emission. In view of this, the doping amount of Ru-PEI for synthesizing Ru-PEI@SiO_2@Au was optimized to be 1.0 mL for the best ECL response (Fig. S5 in Supporting information).

A naked-eye dual-signal output strategy was engaged in ECL test strips for AFB1 detection using Ru-PEI@SiO_2@Au as difunctional probe. As depicted in Fig. 1, AFB1-BSA antigens and mouse-IgG antibodies were preliminarily immobilized on T-line and C-line of ECL test strips. When negative sample without AFB1 target was added onto pad, anti-AFB1 bonded with Ru-PEI@SiO_2@Au probes (anti-AFB1-probe complexes) were captured by AFB1-BSA on T-line to the largest extent. By this time the intensely red colorimetric produced by the plasmonic activity of Au NPs and bright red ECL imaging signals were observed at the T-line zone. Reversely, in the presence of AFB1 target as a positive sample, AFB1 preferentially reacted with anti-AFB1-probe complexes, resulting in lessened anti-AFB1-probe complexes captured on T-line during the lateral flow. Then dual signals readout on T-line could be weakened, which were analyzed by an ImageJ software to quantify the amount of AFB1 targets. [24,25] A red-turned C-line guaranteed accomplishment and effectiveness of the entire testing process. To ensure clear T-line but little background, the optimum anti-AFB1 amount was 0.1 ng/mL (Fig. S6A in Supporting information) to conjugated with probes for further detection. Accordingly, the immunorecognition time of 15 min (Fig. S6B in Supporting information) and the applied constant potential of 1.25 V (Figs. S6C and D in Supporting information) were systematically optimized.

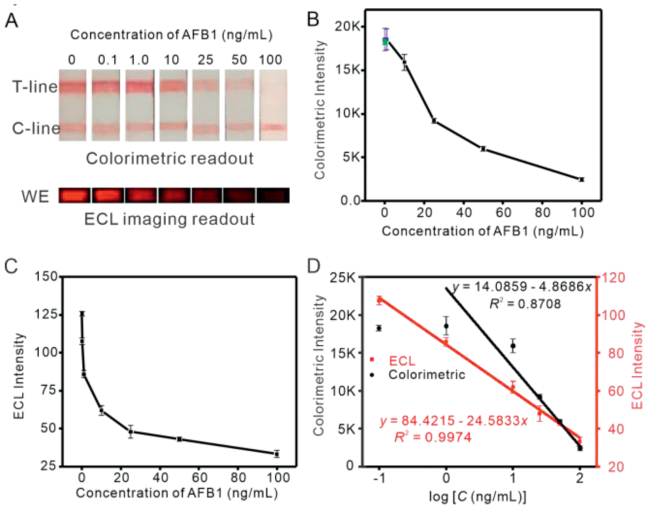

Fig. 4. (A) Colorimetric and ECL imaging photographs of test strips for detection a series concentration of AFB1 standards. The corresponding (B) colorimetric and (C) ECL intensities analyzed by ImageJ. (D) Linear relationships of colorimetric or ECL imaging intensities on the logarithm of the AFB1 concentrations.

ECL test strips were utilized to quantify standard AFB1 samples with increasing concentration. Dual-signal results in Fig. 4A illustrated that the more AFB1 existed, the weaker colorimetric and ECL imaging intensity were simultaneously visible to the naked eye.

But it was remarkable that colorimetric signals were incapable to distinguish AFB1 targets at very low concentrations ranged from 0 to 1.0 ng/mL (Fig. 4B). Under the same conditions, the well-defined ECL images of WE electrodes at T-line zones endowed highly responsive ECL intensities to trace AFB1 targets (Fig. 4C). The gray values of smartphone-recorded ECL images linearly relied on the logarithms of different AFB1 concentrations from 0.1 ng/mL to 100 ng/mL with a favorable correlation coefficient (R^2) of 0.992 (Fig. 4D, red line). For colorimetric assay of AFB1, a linear range from 1.0 ng/mL to 100 ng/mL with R^2 of 0.871 was received (Fig. 4D, black line). The limit of detection (LOD) for ECL imaging and colorimetric mode were 12 pg/mL and 103 pg/mL, respectively. The sensitivity of this ECL test strip was greatly improved for 10-time under the integration of ECL image mode. Upon comparing with previous visualization assays, this ECL test strip had the superior detection sensitivity (Table S1 in Supporting information). Furthermore, under five parallel tests, an RSD of 1.6% for blanks and 2.7% for AFB1 targets were obtained (Fig. 5A), certifying the satisfactory reproducibility of this strips. Besides, several kinds of mycotoxins including OTA, DON and ZEN were individual or mixed with the same level AFB1 targets for sensing detection. A drastically reduced ECL intensity was presented only for AFB1 in Fig. 5B, demonstrating high selectivity and anti-interference for the target. Even after 30 days storage, there was no obvious change in the ECL intensity towards 50 ng/mL of AFB1 (Fig. 5C), manifesting ultrahigh stability of ECL test strips. The total cost of a strip was about ¥3.44/$0.48 (Table S2 in Supporting information).

Corn is a kind of very popular food in our daily life, which is very susceptible to be contaminated by mycotoxins especially AFB1

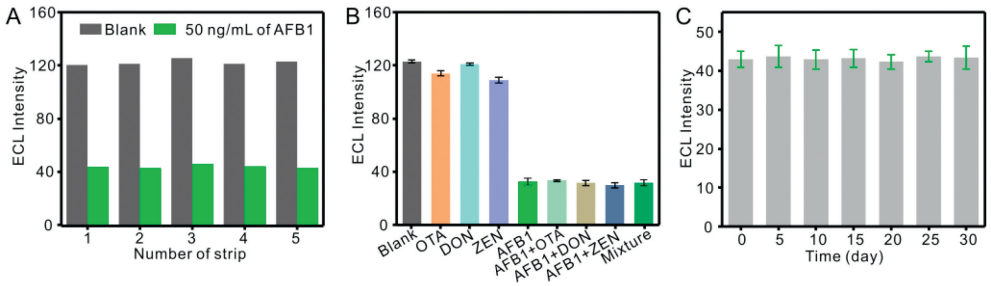

Fig. 5. (A) Reproducibility of five parallel ECL test strips toward 50 ng/mL of AFB1 detection. (B) Selectivity of ECL test strips to different interferents (OTA, DON, ZEN at a concentration of 100 ng/mL and several mixtures). (C) Stability of ECL test strips after 30 days storage.

under improper treatment [26]. In this regard, corn sample was used to validate the practicability of the proposed ECL test strips (Table S3 in Supporting information). Three samples with different concentrations of AFB1 (0.93, 20.03 and 49.82 μg/mL) were prepared by adding AFB1 into corn samples and calibrated by HPLC assay. Then, after diluted 1000-fold for further measurement by the ECL test strips, satisfactory recovery rate of the spiked samples by the colorimetric mode ranged from 96.4 % to 107.0 % with RSD less than 5.5 %. The recovery rate of ECL imaging mode ranged from 99.2 % to 101.7 % with RSD less than 4.9 %, which revealed that the proposed ECL test strips served as a powerful rapid detection tool for AFB1 analysis.

In summary, we constructed a portable ECL imaging test strip for dual-signal visualized detection of AFB1 by integrating a carbon ink-based electrodes system into LFI strips. The colorimetric and ECL imaging signals were trigged by the anti-AFB1-Ru-PEI@SiO_2@Au probes bonded onto the T-line after a competitive immune reaction. Assisted by a smartphone, highly sensitive and selective monitoring of AFB1 level in corn sample was realized. This study sufficiently broadened the detection mode and improved the performance of LFI strips for food safety.

Declaration of competing interest

The authors declare that they have no known competing financial interests or personal relationships that could have appeared to influence the work reported in this paper.

CRediT authorship contribution statement

Miao-Miao Chen: Conceptualization, Project administration, Resources, Writing – original draft, Writing – review & editing. **Min-Ling Zhang:** Data curation, Investigation, Methodology, Project administration. **Xiao Song:** Data curation, Formal analysis, Investigation, Methodology. **Jun Jiang:** Data curation, Investigation, Methodology. **Xiaoqian Tang:** Investigation, Methodology, Software, Validation. **Qi Zhang:** Conceptualization, Methodology, Project administration, Validation. **Xiuhua Zhang:** Methodology, Supervision, Validation. **Peiwu Li:** Conceptualization, Supervision, Validation, Visualization.

Acknowledgments

This work was financially supported by China Postdoctoral Science Foundation (No. 2022T150708), National Key Research and Development Program of China (No. 2023YFF1104600), National Natural Science Foundation of China (Nos. 32072305, 32102089).

Supplementary materials

Supplementary material associated with this article can be found, in the online version, at doi:10.1016/j.cclet.2024.109785.

References

[1] F.P. Guengerich, W.W. Johnson, T. Shimada, et al., Mutat Res. 402 (1998) 121–128.
[2] Q. Zhou, D. Tang, Trends Anal. Chem. 124 (2020) 115814.
[3] Y. Lin, Q. Zhou, D. Tang, et al., Anal. Chem. 88 (2016) 7858–7866.
[4] N.M. Danesh, H.B. Bostan, K. Abnous, et al., Trends Anal. Chem. 99 (2018) 117–128.
[5] Z. Yu, C. Qiu, L. Huang, Y. Gao, D. Tang, Anal. Chem. 95 (2023) 4212–4219.
[6] Y. Lin, Q. Zhou, D. Tang, R. Niessner, D. Knopp, Anal. Chem. 89 (2017) 5637–5645.
[7] S. He, Q. Huang, Y. Zhang, et al., Chin. Chem. Lett. 32 (2021) 1462–1465.
[8] Z. Wei, K. Luciano, X. Xia, ACS Nano 16 (2022) 21609–21617.
[9] G. Xing, W. Zhang, N. Li, Q. Pu, J.M. Lin, Chin. Chem. Lett. 33 (2022) 1743–1751.
[10] X. Tang, Q. Zhang, Z. Zhang, et al., Anal. Chim. Acta 1078 (2019) 142–150.
[11] G. Chen, X. Chen, G. Xu, et al., Food Chem. 412 (2023) 135580.
[12] S. Ren, Q. Li, J. Wang, et al., J. Hazard. Mater. 402 (2021) 123781.
[13] Z. Li, W. Zhang, Q. Zhang, P. Li, X. Tang, ACS Nano 17 (2023) 19359–19371.
[14] L. Yin, T. You, H.R. El-Seedi, et al., Food Chem. 396 (2022) 133707.
[15] L. Wang, X. Wang, L. Cheng, et al., Biosens. Bioelectron. 189 (2021) 113360.
[16] D. Hong, E.J. Jo, K. Kim, M.B. Song, M.G. Kim, Small 16 (2020) 2004535.
[17] D. Hong, K. Kim, E.J. Jo, M.G. Kim, Anal. Chem. 93 (2021) 7925–7932.
[18] P. Nandhakumar, C. Muñoz San Martín, B. Arévalo, et al., ACS Sens. 8 (2023) 3892-3901.
[19] K. Kunpatee, K. Khantasup, K. Komolpis, et al., Biosens. Bioelectron. 242 (2023) 115742.
[20] J.A. Bard, Electrogenerated Chemiluminescence, Marcel Dekker, New York, 2004.
[21] S. Li, Y. Liu, Q. Ma, Trends Anal. Chem. 110 (2019) 277–292.
[22] H. Xu, X. Zhu, J. Wang, Z. Lin, G. Chen, Luminescence 34 (2019) 308–315.
[23] Y. Hou, Y. Fang, Z. Zhou, et al., Adv. Opt. Mater. 11 (2023) 2202737.
[24] J. Shu, Z. Qiu, D. Tang, Anal. Chem. 90 (2018) 9691–9694.
[25] Z. Yu, H. Gong, M. Li, D. Tang, Biosens. Bioelectron. 218 (2022) 114751.
[26] X. Zhang, J. Zhang, X. He, et al., Front. Plant Sci. 8 (2017) 1611.